University of Plymouth

PEARL **https://pearl.plymouth.ac.uk**

Faculty of Science and Engineering School of Engineering, Computing and Mathematics

2007-05

Compositional controls on melting and dissolving a salt into a ternary melt

Hatton, Daniel

http://hdl.handle.net/10026.1/1455

10.1098/rspa.2007.1819
Proc. R. Soc. A
The Royal Society

All content in PEARL is protected by copyright law. Author manuscripts are made available in accordance with publisher policies. Please cite only the published version using the details provided on the item record or document. In the absence of an open licence (e.g. Creative Commons), permissions for further reuse of content should be sought from the publisher or author.

Compositional controls on melting and dissolving a salt into a ternary melt

By D. C. Hatton and A. W. Woods

BP Institute for Multi-Phase Flow, University of Cambridge, Madingley Road, Cambridge CB3 0EZ, UK.

We explore theoretically the controls on dissolution of salt A, in an under-saturated brine of salts A and B. We show that, as the concentration of B increases, the dissolution rate of A decreases, for brine of given temperature. We also show that there is a sharper decrease in dissolution rate with increasing concentration, for concentrations of B above a critical value, where B limits the equilibrium concentration. We explore the implications of the predictions for dissolution of KCl or $NaCl$, by a mixed brine of $NaCl$ and KCl, a common reaction that may arise in dissolution of evaporites. We predict that, with mixed-composition brine, KCl crystals dissolve more rapidly than $NaCl$ crystals, unless the (far-field) brine is nearly saturated in KCl. We also predict that the dissolution rate of these salts is largely independent of fluid temperature, and is controlled by compositional diffusion.

Keywords: dissolution, melting, diffusion, conduction, salt, ice

1. Introduction

There are natural and industrial processes, including salt dissolution during water flooding of porous rocks, melting caused by hot magma intrusion into the shallow crust of the Earth, and solution mining of minerals, in which a soluble solid dissolves into a multi-component liquid solution.

In particular, in the context of evaporite formation and extraction, there is interest in the dissolution of one salt by an aqueous solution containing two or more solutes. The purpose of this paper is to quantify the dissolution rate, as a function of the temperature and the concentration of each salt in the melt. We restrict attention to the situation in which diffusion is the dominant mechanism for heat and mass transport, building from the classical Stefan problem approach for equilibrium phase change (cf. Carslaw & Jaegar, 1986; Woods, 1992). Although in many natural situations, fluid convection may develop, there are régimes in which diffusion provides the dominant mass transport process. For example, as evaporites are formed, there are periods in which relatively fresh fluid may enter a lagoon (cf. Sonnenfeld, 1985). This may then lead to dissolution of salt from the bed of the lagoon, and formation of a stable stratification. Also, in the context of sea ice/ocean interaction, relatively warm, saline ocean water may impinge on the underside of sea ice. The ice may then melt into the ocean water, again forming a stable stratification (cf. van Andel, 1994). In these cases, the phase change will be diffusion-controlled. Even where there is a driving force for convection, our analysis provides a reference, with which to compare the effects of convection on the phase change. In section 3 we build on the self-similar solutions for dissolution of a single species in a brine

developed by Woods (1992). We focus on the effect of a second salt in solution. We thereby identify (sections 4, 5) some of the controls exerted by fluid concentration and temperature on the dissolution rate.

2. The model

Figure 1 is a schematic of our model system, in which we indicate that the compositional boundary layers, adjacent to the dissolving solid, are much thinner than the thermal boundary layer, owing to the much smaller value of compositional diffusivity $O\left(10^{-9}\,\mathrm{m^2\,s^{-1}}\right)$, compared to the thermal diffusivity $O\left(10^{-6}\,\mathrm{m^2\,s^{-1}}\right)$.

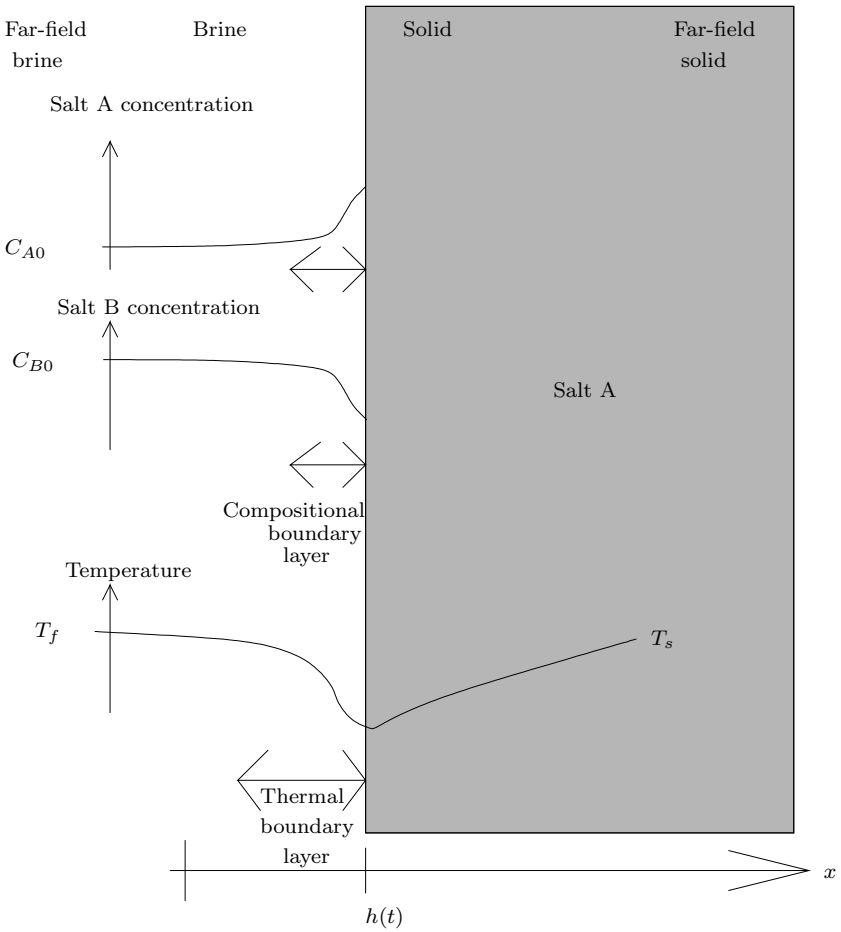

Figure 1. This is a schematic of our model system, with cartoon plots of the spatial variation of concentrations and temperature. In this example, the solid is pure salt A, the far-field brine contains some salt B, and the two far-field temperatures are similar.

In modelling equilibrium dissolution of one salt into a brine of two salts, we first describe conservation of the mass of each salt and conservation of heat in the liquid. We then model heat and salt conservation across the ablating interface. As

solid dissolves into the brine, the concentration of the dissolving salt in the liquid increases; meanwhile, as the solid vacates space, the other salt can diffuse to fill that space only if there is a concentration gradient for it to descend, depressing the concentration of that salt near the interface. Both salts, therefore, diffuse in the liquid; this is important, since the equilibrium condition at the interface depends on both salt concentrations.

(*a*) *Governing equations*

We now develop a quantitative model for mass and heat conservation. If a unit volume of the brine contains a mass m_W of water, m_A of salt A and m_B of salt B, then we denote the concentrations of A and B by:

$$C_A = \frac{m_A}{m_A + m_B + m_W}; \tag{2.1}$$

$$C_B = \frac{m_B}{m_A + m_B + m_W}. \tag{2.2}$$

Each salt may diffuse through the liquid. In general, the salts have different diffusion coefficients, which depend on the concentration of the other salt, but in the dilute limit, which, for simplicity, we assume applies herein, we take them to be constants D_A for salt A and D_B for salt B, leading to conservation equations:

$$\frac{\partial C_A}{\partial t} - v\frac{\partial C_A}{\partial x} = D_A \frac{\partial^2 C_A}{\partial x^2}; \tag{2.3}$$

$$\frac{\partial C_B}{\partial t} - v\frac{\partial C_B}{\partial x} = D_B \frac{\partial^2 C_B}{\partial x^2}, \tag{2.4}$$

where we have, in a Boussinesq approximation, neglected the effects of variation in the density of the fluid, $\rho_L \equiv m_A + m_B + m_W$. Once this is done, conservation of water (within the fluid) is automatically satisfied by conserving the two salts. v is a spatially-uniform fluid speed, in the negative x direction, whose origin will be made clear in the discussion of equation 2.9. Heat conduction through the liquid ($j = L$) and solid ($j = S$) involves the thermal diffusivity, κ_j:

$$\frac{\partial T}{\partial t} - v\frac{\partial T}{\partial x} = \kappa_j \frac{\partial^2 T}{\partial x^2}. \tag{2.5}$$

Usually, we consider the dissolving solid to be composed of salt A, but our model formulation can also handle either salt B or ice as the dissolving solid.

(*b*) *Phase equilibrium and saturation*

We assume the concentration of the liquid in contact with the solid interface is given by the phase-equilibrium value. This has the form shown in figure 2, which corresponds to the *KCl-NaCl* system. Each contour corresponds to the equilibrium concentrations for a given temperature. If the brine contains a second salt, then the equilibrium concentration of the dissolving phase, for a given temperature, decreases. Furthermore, as the concentration of the second salt increases beyond a critical point (the kink in each contour of figure 2b,) there is a rapid decrease

in the equilibrium concentration of the dissolving salt. For convenience, we use a simplified form for this equilibrium surface, given by

$$\begin{aligned} T &= \max\left(a_A C_A + b_A C_B - c_A,\right. \\ &\quad \left. a_B C_A + b_B C_B - c_B, a_I C_A + b_I C_B - c_I\right), \end{aligned} \tag{2.6}$$

where a_i, b_i and c_i are parameters obtained by fitting to the empirical data reproduced in figure 2a. The best-fit values are tabulated in the left-hand part of table 1. This model approximates the equilibrium surface by three planes, intersecting at linear boundaries, which divide the concentration space into three régimes: the high A concentration régime (equilibrium with solid A,) where a_A, b_A, and c_A are relevant, the "A-dominated branch," the high B concentration régime, (equilibrium with solid B,) where a_B, b_B, and c_B are relevant, the "B-dominated branch," and the low concentration régime (equilibrium with solid ice,) where a_I, b_I, and c_I are relevant, the "ice-dominated branch." Our description (equation 2.6) could be seen as a linearized, local approximation to the high-order polynomials that it is traditional (cf. Hall *et al.*, 1988; Sterner *et al.*, 1988) to fit to the equilibrium data.

Figure 3 illustrates the importance of the equilibrium surface in figure 2: the condition of the fluid at the dissolving interface is constrained to lie on that surface.

(*c*) *Interfacial boundary conditions*

At the interface, we require conservation of A, B, and heat. If the interface has position $h(t)$ at time t, then heat conservation across the interface requires

$$\kappa_L \left.\frac{\partial T}{\partial x}\right|_{x=h(t)-} = \kappa_S \left.\frac{\partial T}{\partial x}\right|_{x=h(t)+} - l_k h'(t), \tag{2.7}$$

where the subscript k indexes the solid composition: $k = A$ for salt A, $k = B$ for salt B, or $k = I$ for ice; in our numerical and graphical examples, and in our qualitative conclusions, we examine only solid salts, $k \in \{A, B\}$, but our algebraic expressions are also valid for ice, $k = I$. l_k is the ratio of the specific latent heat of dissolution of material k to its specific heat capacity. Also, the temperature is continuous across the interface:

$$T|_{x=h(t)-} = T|_{x=h(t)+}. \tag{2.8}$$

Conservation of A across the interface requires

$$\rho_L D_A \left.\frac{\partial C_A}{\partial x}\right|_{x=h(t)-} + \rho_L \, C_A|_{x=h(t)-} \left(h'(t) + v\right) = \rho_S \delta_{kA} h'(t), \tag{2.9}$$

where δ_{kl} is the Kronecker delta: $\delta_{kl} = 1$ where $k = l$, $\delta_{kl} = 0$ where $k \neq l$, and v is the (spatially-uniform) fluid speed, away from the interface, required to allow for volume expansion on phase change, associated with the differing densities ρ_L of the liquid and ρ_S of the solid (cf. Chiareli & Worster, 1995). Similarly, conservation of B across the interface requires

$$\rho_L D_B \left.\frac{\partial C_B}{\partial x}\right|_{x=h(t)-} + \rho_L \, C_B|_{x=h(t)-} \left(h'(t) + v\right) = \rho_S \delta_{kB} h'(t). \tag{2.10}$$

Because the solid and liquid have different densities, we also account for the conservation of total mass:

$$\rho_L \left(h'(t) + v\right) = \rho_S h'(t). \tag{2.11}$$

We can substitute from equation 2.11 into equations 2.9 and 2.10, to give:

$$r_{LS} D_A \left.\frac{\partial C_A}{\partial x}\right|_{x=h(t)-} + C_A|_{x=h(t)-} h'(t) = \delta_{kA} h'(t); \tag{2.12}$$

$$r_{LS} D_B \left.\frac{\partial C_B}{\partial x}\right|_{x=h(t)-} + \rho_L \, C_B|_{x=h(t)-} h'(t) = \delta_{kB} h'(t), \tag{2.13}$$

where r_{LS} is the density ratio ρ_L/ρ_S.

3. Self-similar solutions

(*a*) *The form of the solutions*

Guided by the results of Woods (1992), who presented self-similar solutions for a single salt, we have developed analogous solutions for the ternary system. We express solutions in terms of the error function

$$G(z) = \int_{u=-\infty}^{z} g(u)\,\mathrm{d}u, \tag{3.1}$$

where the normalized Gaussian

$$g(u) = \frac{\exp\left(-u^2/2\right)}{\sqrt{2\pi}}. \tag{3.2}$$

The solutions depend on x and t only through the dimensionless similarity variable

$$\eta = \frac{x}{\sqrt{2D_A t}}. \tag{3.3}$$

By analogy to this variable, we define a time-independent boundary position in η space (and dissolution rate constant)

$$\lambda = \frac{h(t)}{\sqrt{2D_A t}} = \frac{\sqrt{2t}\dot{h}(t)}{\sqrt{D_A}}. \tag{3.4}$$

(i) *The fluid region*

We consider first the fluid region of the system, to the left of the boundary (figure 1.) Here, the solutions are:

$$C_A = C_{A0} + \Delta C_A G(\xi); \tag{3.5}$$

$$C_B = C_{B0} + \Delta C_B G(R\xi); \tag{3.6}$$

and

$$T = T_f + \Delta T_L G(K_L \xi). \tag{3.7}$$

The governing equations suggest $R = \sqrt{D_A/D_B}$ and $K_L = \sqrt{D_A/\kappa_L}$ are key dimensionless numbers. ΔC_A, ΔC_B, and ΔT_L remain to be determined. The variable $\xi = \eta + (1/r_{LS} - 1)\,\lambda$ represents a translation of the similarity variable η, adjusted to allow for advection of salt and heat by the fluid velocity $-v$. These solutions satisfy equations 2.3 and 2.4, and the fluid version of equation 2.5, as well as the far-field conditions (figure 1.)

(ii) *The solid region*

Next, we turn to the solid region, to the right of the boundary (figure 1.) Here, only temperature is relevant, and the solution is

$$T = T_s + \Delta T_S\,(G\,(K_S\eta) - 1)\,. \tag{3.8}$$

The governing equations suggest $K_S = \sqrt{D_A/\kappa_S}$ is a key dimensionless number. ΔT_S remains to be determined. This solution satisfies the solid version of equation 2.5, as well as the far-field conditions (figure 1.)

(*b*) *Constraints on the solutions from boundary conditions*

(i) *Boundary between a fluid region and a solid region*

Substituting equation 3.5 into equation 2.12 gives

$$\Delta C_A = \frac{(\delta_{kA} - C_{A0})\,\lambda/r_{LS}}{g\,(\lambda/r_{LS}) + (\lambda/r_{LS})\,G\,(\lambda/r_{LS})}. \tag{3.9}$$

The concentration gradient, driving diffusion of salt A away from the boundary, is controlled by the competition between a term representing supply of salt A from the dissolving solid, and a term representing the uptake of salt A by the newly-liquid volume. By a similar analysis based on equations 2.13 and 3.6,

$$\Delta C_B = \frac{(\delta_{kB} - C_{B0})\,R\lambda/r_{LS}}{g\,(R\lambda/r_{LS}) + (R\lambda/r_{LS})\,G\,(R\lambda/r_{LS})}. \tag{3.10}$$

Substituting equation 3.7 into equation 2.7 gives

$$\Delta T_L = \frac{K_L\,(\Delta T_S g\,(K_S\lambda) - l_k K_S\lambda)}{K_S g\,(K_L\lambda/r_{LS})}, \tag{3.11}$$

while substituting equation 3.7 into equation 2.8 gives

$$\Delta T_S = \frac{K_S\,((T_s - T_f)\,g\,(K_L\lambda/r_{LS}) + l_k K_L\lambda G\,(K_L\lambda/r_{LS}))}{K_L g\,(K_S\lambda)\,G\,(K_L\lambda/r_{LS}) + K_S\,(1 - G\,(K_S\lambda))\,g\,(K_L\lambda/r_{LS})}. \tag{3.12}$$

The heat fluxes, driven by the temperature gradients on either side of the boundary, differ by the uptake of latent heat in dissolution.

(*c*) *Constraints on the solutions from the equilibrium conditions*

(i) *Boundary between an all-fluid region and an all-solid region*

At the boundary, equation 2.6 applies, i.e.

$$T_s + \Delta T_S\,(G\,(K_S\lambda) - 1) = a_i\left(C_{A0} + \Delta C_A G\left(\frac{\lambda}{r_{LS}}\right)\right) + b_i\left(C_{B0} + \Delta C_B G\left(\frac{R\lambda}{r_{LS}}\right)\right) - c_i. \tag{3.13}$$

Substituting ΔT_S from equation 3.12 into equation 3.13,

$$\begin{aligned} T_f &= \frac{\left(a_i\left(C_{A0}+\Delta C_A G\left(\lambda/r_{LS}\right)\right)+b_i\left(C_{B0}+\Delta C_B G\left(R\lambda/r_{LS}\right)\right)-c_i-T_s\right)}{K_S\left(1-G\left(K_S\lambda\right)\right)g\left(K_L\lambda/r_{LS}\right)} \\ &\quad\times\left(K_L g\left(K_S\lambda\right)G\left(K_L\lambda/r_{LS}\right)+K_S\left(1-G\left(K_S\lambda\right)\right)g\left(K_L\lambda/r_{LS}\right)\right) \\ &\quad+\frac{l_k K_L\lambda G\left(K_L\lambda/r_{LS}\right)}{g\left(K_L\lambda/r_{LS}\right)}+T_s. \end{aligned} \tag{3.14}$$

Equation 3.14 pertains to the i-dominated branch of equation 2.6; to choose whether i is "A," "B," or "ice," given C_{A0}, C_{B0}, and λ, we calculate the concentrations $C_{A0}+\Delta C_A G\left(\lambda/r_{LS}\right)$ and $C_{B0}+\Delta C_B G\left(R\lambda/r_{LS}\right)$ at the boundary, and choose the i value in whose concentration-space domain the boundary concentrations fall. Equation 3.14, which we term the "dispersion relation," is an implicit determination of λ, and is the key result of this paper.

4. Discussion

We have solved the dispersion relation for a range of cases, to illustrate how the rate of dissolution behaviour depends on the concentration of each salt in the brine.

First, we consider the solid to be pure KCl, and we explore (section a) the effect of changing the $NaCl$ concentration in the fluid on the dissolution rate. We contrast this to the rate of dissolution of solid $NaCl$ in the same fluid conditions (section b,) to illustrate the impact of the presence of two salts in solution. We also show (sections a, b) that variations in the temperature of the fluid have a much smaller effect. This results from the equilibrium constraint at the interface, combined with diffusion of solute. Similar results are found in all problems considered in this work. We then (section c) generalize the results, allowing the far-field fluid to contain both $NaCl$ and KCl. We explore how the dissolution rates of $NaCl$ and KCl vary in this two-salt brine. To these ends, we choose parameters suitable for a system where salt A is KCl, and salt B is $NaCl$ (for clarity about the substances involved, we will henceforth use subscripts K and N, not A and B.) The parameter values can be found in the right-hand part of table 1.

(*a*) *Dissolution of solid KCl by NaCl brine*

In figure 4, we plot predictions for the dissolution rate of solid KCl ($k=K$,) as a function of $NaCl$ concentration in the far-field brine. Three curves are plotted, corresponding to far-field brines at $T_f=-10\,^\circ\mathrm{C}$, $T_f=50\,^\circ\mathrm{C}$, and $T_f=110\,^\circ\mathrm{C}$. All of these temperatures are well below the melting point of the salt (into pure liquid salt.) The T_f variation is deliberately extreme, and is purely an input to produce model conclusions: the intention is that if we predict that, owing to the strong dependence of equilibrium temperature on fluid concentration, the dissolution rate is insensitive to this extreme temperature variation, then it will be even more insensitive to smaller, more geophysically realistic temperature variations. Exactly what is "geophysically realistic" will depend on the details of the application. However, the existence of thermal contact between fluid and solid at the interface does not, in itself, prohibit large temperature contrasts between the far-field fluid and the far-field solid, where "far-field" means the distance from the interface is large, compared with the (time-dependent) characteristic length for thermal conduction.

Addition of extra $NaCl$ to the far-field brine reduces the dimensionless KCl dissolution rate significantly, from a maximum value of ~ 0.15 at $C_{N0} = 0$. This decrease in dissolution rate becomes abruptly more rapid when C_{N0} passes a value we term the *critical concentration* (point X, $C_{N0} = 0.26$, $T_f = 50\,^{\circ}\mathrm{C}$, $\lambda = 0.047$.) Eventually, at some higher C_{N0} (point Y, $C_{N0} = 0.28$, $T_f = 50\,^{\circ}\mathrm{C}$, $\lambda = 0$,) dissolution stops altogether. Later in this section, we will provide physical interpretations of the critical concentration and the stoppage-of-dissolution concentration. As the far-field brine temperature increases by 120 K, these two concentrations do not change perceptibly. The effect of changing the far-field brine temperature on the dissolution rate is smaller than that of changing the far-field $NaCl$ concentration: even the enormous temperature shift between the highest and lowest contours changes the dissolution rate by only ~ 0.011 below the critical concentration, and by only ~ 0.008 between the critical concentration and the stoppage-of-dissolution concentration.

To help interpret the variation of dissolution rate with concentration (figure 4,) we now illustrate how the concentration and temperature of the liquid adjust from the far-field to the interface, in three specific cases, A ($C_{N0} = 0$, $T_f = 50\,^{\circ}\mathrm{C}$, $\lambda = 0.14$,) B ($C_{N0} = 0.12$, $T_f = 50\,^{\circ}\mathrm{C}$, $\lambda = 0.10$,) and C ($C_{N0} = 0.27$, $T_f = 50\,^{\circ}\mathrm{C}$, $\lambda = 0.03$,) as marked on figure 4. To this end, in figure 5a, we plot predicted KCl concentration-$NaCl$ concentration profiles of the brine, for three far-field brine $NaCl$ concentrations (points A, B, and C in figure 4,) along with the predicted locus, in KCl concentration-$NaCl$ concentration space, of interface brine conditions, as C_{N0} varies. Similarly, in figure 5b, we plot predicted KCl concentration-temperature profiles of the brine, for three far-field brine $NaCl$ concentrations (points A, B, and C in figure 4,) along with the predicted locus, in KCl concentration-temperature space, interface brine conditions, as C_{N0} varies.

Increasing the far-field $NaCl$ concentration decreases the interface KCl concentration, and therefore decreases the KCl flux from the interface to the far-field brine, as indeed it must, to be associated with the reduced KCl dissolution rate we have described. In addition, as the far-field brine $NaCl$ concentration increases, the interface temperature increases. This reduces the heat flux to the interface, from both far fields. Again, this is necessary, for the increase in far-field brine $NaCl$ concentration to be associated with a decrease in dissolution rate, given a fixed latent heat. In figure 5a, one can see that the critical concentration (point X) is associated with the interface brine conditions switching from the KCl-dominated to the $NaCl$-dominated branch of equation 2.6. On the $NaCl$-dominated branch, the reduction of interface brine KCl concentration, as the far-field and interface brine $NaCl$ concentrations increase, is quicker than on the KCl-dominated branch ($b_N/a_N > b_K/a_K$,) as one would expect, given the associated rapid reduction of dissolution rate. The stoppage-of-dissolution concentration (point Y) is associated with the far-field brine being saturated in $NaCl$, and therefore unable to dissolve any KCl. Intriguingly (figure 5a,) where there is $NaCl$ in the far-field fluid, the $NaCl$ concentration in the fluid varies with position (and therefore with time.) This is necessary for dissolution, because, as the dissolution front passes by a given location, it replaces solid material, consisting entirely of KCl, with liquid, containing $NaCl$. Since the $NaCl$ flux is zero in the solid, there has to be a non-zero flux, and therefore an $NaCl$ concentration gradient, in the fluid adjacent to the front, in order that the newly-formed fluid element, produced by the dissolution, has a non-zero

$NaCl$ content. This transport also serves to reduce the magnitude of the $NaCl$ concentration gradient, by spreading out the constant far-field/dissolution-front concentration contrast (the latter concentration being fixed by phase equilibrium) over the system's increasing length scale.

To help interpret the variation of dissolution rate with temperature (figure 4,) we now illustrate how the concentration and temperature of the liquid adjust from the far-field to the interface in three specific cases, D ($C_{N0} = 0.12$, $T_f = -10\,^\circ$C, $\lambda = 0.097$,) B, and E ($C_{N0} = 0.12$, $T_f = 110\,^\circ$C, $\lambda = 0.11$,) as marked on figure 4. To this end, in figure 6a, we plot predicted KCl concentration-temperature profiles of the brine, for three far-field brine temperatures (points D, B, and E in figure 4,) along with the predicted locus, in KCl concentration-temperature space, of interface brine conditions, as T_f varies. Similarly, in figure 6b, we plot predicted KCl concentration-$NaCl$ concentration profiles of the brine, for three far-field brine temperatures (points D, B, and E in figure 4,) along with the predicted locus, in KCl concentration-$NaCl$ concentration space, of the interface brine conditions, as T_f varies.

The KCl concentration-$NaCl$ concentration profiles for the three far-field brine temperatures are almost identical. The increase in interface KCl concentration, and therefore in KCl flux from the interface to the far-field brine, on increasing the far-field brine temperature, is tiny. This is consistent with the weak dependence of dissolution rate on far-field brine temperature. The decrease in interface $NaCl$ concentration, and the attendant increase in $NaCl$ flux from the far-field brine to the interface, on increasing the far-field brine temperature, is similarly small. However, the increase in interface temperature, as the far-field brine temperature increases, is substantial, albeit smaller than the increase in far-field brine temperature. Even though the change in concentration is small, a relatively large change in temperature is required, in order to maintain equilibrium, because the rate of change of the equilibrium temperature with concentration is so large ($a_K = 860\,$K, $b_K = 640\,$K.) As far-field brine temperature increases, interface temperature also increases, so that part of the heat flux from the brine to the interface can be balanced by a heat flux from the interface to the solid, and vice versa: for the coldest far-field fluid temperature, there is more heat flux from the far-field solid to the interface than is needed to supply latent heat, and the need to transport away excess heat to the far-field fluid leads to an interface temperature higher than the far-field fluid temperature. The rate of dissolution is limited by the requirement to remain in equilibrium: therefore, as the temperature difference between the far-field brine and the far-field solid increases, a progressively smaller fraction of the heat flux to the interface is used to supply the latent heat of dissolution. This effect is shown in figure 7, where it is clear that, except in a narrow range of far-field brine temperatures, close to the far-field solid temperature, the heat flux r, used as latent heat of dissolution, is a tiny fraction of the heat flux q, delivered to the interface by the brine. This explanation of the minor importance of temperature, relative to concentration, relies on the liquidus being steep (large values of a_k and b_k, compared with the available range of temperatures.) For solids other than KCl (and $NaCl$,) the liquidus may be shallower, and temperature may be more important; in particular, for solid ice, $a_I = -44.0\,$K and $b_I = -122.7\,$K. One might, therefore, expect the influence of temperature on dissolution rate, relative to that of $NaCl$ concentration, to be ~ 5 times greater for solid ice, than for solid KCl.

In figure 6a, the spatial variation of temperature, for $T_f = 50\,^\circ\mathrm{C}$, is almost invisible, for two reasons. Firstly, it is small compared with the imposed variation of far-field fluid temperature, while the latter determines the range of the vertical axis. Secondly, the temperature variation happens over a much larger distance scale than the spatial concentration variation, so that almost all the temperature variation is compressed at the left-hand end of this graph, with concentration at its extreme low value. The same brine profile is presented in a different way, in figure 8, where we plot temperature as a function of dimensionless position, for $T_f = 50\,^\circ\mathrm{C}$, which eliminates both causes of near-invisibility of the spatial temperature variation.

Interface temperature is not strongly constrained by phase equilibrium, because the phase-equilibrium relations are so steep that a tiny adjustment of concentration can maintain phase equilibrium through a huge range of temperatures. The leading-order contribution to interface temperature is a weighted average of the two far-field temperatures, just as if heat were being conducted from the hotter far field to the colder far field without any intervening phase-change front. The different thermal conductivities of $NaCl$ and KCl lead to a small difference in the weightings. The dissolution introduces a second-order contribution to interface temperature, through the need to drive heat flux into the interface to supply latent heat. This second-order contribution will be smaller than the leading-order contribution, because the latent heat of dissolution is small compared with the through-going heat flux (unless the two far-field temperatures are exceptionally close together; cf. figure 7.)

(*b*) *Dissolution of solid KCl or solid NaCl, by NaCl brine*

In figure 9, we compare predictions (cf. figure 4,) for the dissolution rate of solid KCl ($k = K$,) as a function of $NaCl$ concentration in the far-field brine, with predictions for the dissolution rate of solid $NaCl$ ($k = N$,) as a function of $NaCl$ concentration in the far-field brine. For each solid, three curves are plotted, corresponding to far-field brines at $T_f = -10\,^\circ\mathrm{C}$, $T_f = 50\,^\circ\mathrm{C}$, and $T_f = 110\,^\circ\mathrm{C}$.

The dissolution rate for solid $NaCl$ decreases with increasing far-field $NaCl$ concentration, reaching zero around the same concentration as for solid KCl. However, for solid $NaCl$, there is no critical concentration, i.e. no sudden change in the gradient of λ, with respect to C_{N0}, owing to the lack of any KCl in the system. The effect of changing the far-field brine temperature on the dissolution rate is even smaller for solid $NaCl$ than for solid KCl, with the dimensionless $NaCl$ dissolution rate changing by only ~ 0.0014, over the range of accessible temperatures. For all far-field conditions with $C_{K0} = 0$, the dissolution rate for solid KCl is quicker than that for solid $NaCl$. To understand this, first imagine that the dissolution rates for the two solids, with identical far-field conditions, were the same. To transport away the salt that is transferred from the solution into the brine, the $NaCl$ concentration difference, between the interface and the far-field brine, in the case with solid $NaCl$, must be about the same as the KCl concentration difference, between the interface and the far-field brine, in the case with solid KCl. However, because $b_N = 4876\,\mathrm{K}$ is much larger than $a_K = 860\,\mathrm{K}$, the interface temperature required for phase equilibrium will be higher in the case with solid $NaCl$ (and a high $NaCl$ concentration in the brine at the interface) than in the case with solid KCl (and a high KCl concentration in the brine at the interface.) This raised interface temperature will

reduce the temperature gradient and hence heat flux supplied from the hotter far field to the interface, and increase the temperature gradient and hence heat flux supplied from the interface to the colder far field, thereby reducing the difference in these fluxes which is available as latent heat for dissolution, by a greater margin than can be compensated by the smaller specific latent heat of $NaCl$: this is incompatible with the proposal that the dissolution rates for the two solids are the same, and we deduce that solid $NaCl$ must dissolve more slowly than solid KCl.

To help interpret the variation of $NaCl$ dissolution rate with concentration (figure 9,) we now illustrate how the concentration and temperature of the liquid adjust from the far-field to the interface in three specific cases, F ($C_{N0} = 0$, $T_f = 50\,^{\circ}\mathrm{C}$, $\lambda = 0.1096$,) G ($C_{N0} = 0.12$, $T_f = 50\,^{\circ}\mathrm{C}$, $\lambda = 0.0687$,) and H ($C_{N0} = 0.27$, $T_f = 50\,^{\circ}\mathrm{C}$, $\lambda = 0.0064$,) as marked on figure 9. To this end, in figure 10, we plot predicted $NaCl$ concentration-temperature profiles of the brine, for three far-field brine $NaCl$ concentrations (points F, G, and H in figure 9.)

As far-field brine $NaCl$ concentration increases, interface $NaCl$ concentration remains stubbornly constant; therefore, the concentration difference between the interface and the far-field brine decreases, as does the $NaCl$ flux from the interface to the far-field brine, as indeed it must, to be associated with a reduced $NaCl$ dissolution rate. Simultaneously, the interface temperature increases noticeably, as permitted by the very steep ($b_N = 4876\,\mathrm{K}$) liquidus, suppressing the temperature difference between both far fields and the interface, and therefore the heat flux from both far fields to the interface, which, again, is necessary for the reduced dissolution rate. The interface $NaCl$ concentrations are, unsurprisingly, higher than those where the solid is KCl, which, given the steepness of the liquidus, means that the interface temperatures are a great deal higher than those where the solid is KCl; this latter fact makes for much lower heat fluxes than those where the solid is KCl, and is therefore consistent with dissolution rates being lower for solid $NaCl$ than for solid KCl, even though KCl has the greater latent heat.

(*c*) *Dissolution of solid KCl or solid NaCl, by a mixed brine*

The effect on the dissolution rate, of including KCl in the far-field brine, is illustrated in figure 11. Low to moderate far-field KCl concentrations suppress the dissolution rate, neither much distorting the form of its C_{N0}-dependence, nor greatly affecting the differences between solid KCl and solid $NaCl$. However, for the highest far-field KCl concentration, $C_{K0} = 0.2$, the dispersion curves have crossed over, so that $NaCl$ dissolves more quickly than KCl.

5. Conclusions

We have developed and explored an equilibrium model, for dissolution of a pure solid into a multi-component brine. We have focused on the KCl-$NaCl$-H_2O system, and have developed a family of similarity solutions, which capture the dominant controls on the dissolution, associated with the temperatures of the solid and brine, with the identity (KCl or $NaCl$) of the solid, and, most importantly, with the concentrations of $NaCl$ and KCl in the far-field brine, relative to the equilibrium concentrations at the brine/solid interface.

We found that: where the KCl-dominated branch of the equilibrium surface pertains (as it usually does for solid KCl,) the fractional change in KCl dissolution rate with temperature, over the full ($\sim 120\,\mathrm{K}$) range of temperatures studied, is of order 11 %, while the fractional change in KCl dissolution rate with concentration (of either salt,) over the full (~ 0.2) range of accessible concentrations, is of order 100 %. This implies that concentration is an order of magnitude more important than temperature. Where the $NaCl$-dominated branch pertains (as it usually does for solid $NaCl$,) the fractional change in $NaCl$ dissolution rate with temperature, over the full ($\sim 120\,\mathrm{K}$) range of temperatures studied, is of order 2 %, while the fractional change in $NaCl$ dissolution rate with concentration (of either salt,) over the full (~ 0.28) range of accessible concentrations, is of order 200 %. This implies that concentration is two orders of magnitude more important than temperature. To recap: for both solids, under this study's assumptions of equilibrium dissolution with diffusive transport, we predict the dissolution rates to be approximately independent of far-field brine temperature, in the range $-10\,^{\circ}\mathrm{C}$–$110\,^{\circ}\mathrm{C}$.

In addition to the predictions for the relative importance of concentration and temperature, the calculations show that, with the same far-field conditions, $NaCl$ dissolves more slowly than KCl (unless the far-field brine is very close to saturation in KCl.) This is especially interesting, since it implies that, with a mixed solid, dissolution (in the early-time limit) will tend to produce a partially dissolved zone, in which solid $NaCl$ co-exists with a brine, containing both dissolved $NaCl$ and dissolved KCl. The scenario with a mixed solid is the subject of further study.

This model can be applied directly to other salts, by finding appropriate parameter values for those salts, to replace the $KCl/NaCl$ values presented in table 1, and substituting those values into the algebraic equations presented herein. The possibility of this simple substitution is a key advantage of the analytical method we have adopted, compared with numerical solution of the differential equations.

Acknowledgements

We would like to thank Rio Tinto, for financial support.

References

Carslaw, H. S. & Jaegar, J. C. 1986 *Conduction of Heat in Solids*. Oxford University Press.

Chiareli, A. O. P. & Worster, M. G. 1995 Flow focusing instability in a solidifying mushy layer. *J. Fluid Mech.* **297**, 293–305.

Clauser, C. & Huenges, E. 1995 Thermal conductivity of rocks and minerals. In *Rock Physics and Phase Relations: A Handbook of Physical Constants* (ed. Ahrens, T. J.), chap. 3-9, pp. 105–126. No. 3 in AGU Reference Shelf, Washington, DC: American Geophysical Union.

Hall, D. L., Sterner, S. M. & Bodnar, R. J. 1988 Freezing point depression of $NaCl$-KCl-H_2O solutions. *Econ. Geol.* **83**(1), 197–202.

Lewis[Peggs], S. L. 1995 Densities. In Noyes *et al.* (1995), chap. 2.2.1, pp. 41–43. URL: ⟨`http://www.kayelaby.npl.co.uk/general_physics/2_2/2_2_1.html`⟩.

Linke, W. F. 1965 *Solubilities of Inorganic and Metal-Organic Compounds: A Compilation of Solubility Data from the Periodical Literature*, vol. II: K–Z. Fourth edn. Washington, DC: American Chemical Society. A Revision and Continuation of the Compilation Originated by Atherton Seidell, Ph.D., U. S. National Institutes of Health.

Marliacy, P., Hubert, N., Schuffenecker, L. & Solimando, R. 1998 Use of Pitzer's model to calculate thermodynamic properties of aqueous electrolyte solutions of $Na_2SO_4 + NaCl$ between 273.15 and 373.15 K. *Fluid Phase Equilibr.* **148**(1–2), 95–106.

McGlashan, M. L. 1995a Chemical thermodynamics. In Noyes *et al.* (1995), chap. 3.10, pp. 338–357. Originally compiled by G. W. C. Kaye O.B.E., M.A., D.Sc., F.R.S. and T. H. Laby M.A., Sc.D., F.R.S.; now prepared under the direction of an editorial committee. URL: ⟨`http://www.kayelaby.npl.co.uk/`⟩.

McGlashan, M. L. 1995b Properties of solutions. In Noyes *et al.* (1995), chap. 3.6, pp. 266–271. Originally compiled by G. W. C. Kaye O.B.E., M.A., D.Sc., F.R.S. and T. H. Laby M.A., Sc.D., F.R.S.; now prepared under the direction of an editorial committee. URL: ⟨`http://www.kayelaby.npl.co.uk/`⟩.

Morrell, R. 1995 Thermal conductivities. In Noyes *et al.* (1995), chap. 2.3.7, pp. 81–94. URL: ⟨`http://www.kayelaby.npl.co.uk/general_physics/2_3/2_3_7.html`⟩.

Noyes, J. G., Asher, J., Jones, O. C. & Phillips, G. F. (eds.) 1995 *Kaye & Laby: Tables of Physical and Chemical Constants*. Sixteenth edn. Harlow: Longman. Originally compiled by G. W. C. Kaye O.B.E., M.A., D.Sc., F.R.S. and T. H. Laby M.A., Sc.D., F.R.S.; now prepared under the direction of an editorial committee. URL: ⟨`http://www.kayelaby.npl.co.uk/`⟩.

Phillips, G. F. 1995a Properties of the elements. In Noyes *et al.* (1995), chap. 3.1.2, pp. 212–215. URL: ⟨`http://www.kayelaby.npl.co.uk/chemistry/3_1/3_1_2.html`⟩.

Phillips, J. G. E. 1995b Properties of inorganic compounds. In Noyes *et al.* (1995), chap. 3.2, pp. 223–238. URL: ⟨`http://www.kayelaby.npl.co.uk/chemistry/3_2/3_2.html`⟩.

Ramos, R., Gaisford, S., Buckton, G., Royall, P. G., Yff, B. T. S. & O'Neill, M. A. A. 2005 A comparison of chemical reference materials for solution calorimeters. *Int. J. Pharm.* **299**(1–2), 73–83.

Richardson, M. J. 1995 Specific heat capacities. In Noyes *et al.* (1995), chap. 2.3.6, pp. 76–81. URL: ⟨`http://www.kayelaby.npl.co.uk/general_physics/2_3/2_3_6.html`⟩.

Sonnenfeld, P. 1985 Occurrence of potash beds within evaporite basins. In *Proceedings of the Symposium Solution Mining of Salts and Brines* (eds. Schlitt, W. J. & Larson, W. C.), pp. 113–117. Society of Mining Engineers, New York: Society of Mining Engineers.

Sterner, S. M., Hall, D. L. & Bodnar, R. J. 1988 Synthetic fluid inclusions. v. solubility relations in the system $NaCl$-KCl-H_2O under vapor-saturated conditions. *Geochim. Cosmochim. Acta* **52**(5), 989–1005.

van Andel, T. H. 1994 *New Views on an Old Planet: A History of Global Change*. Second edn. Cambridge: Cambridge University Press.

Wheeler, D. R. & Newman, J. 2004 Molecular dynamics simulations of multicomponent diffusion: 1. equilibrium method. *J. Phys. Chem. B* **108**(47), 18353–18361.

Woods, A. W. 1992 Melting and dissolving. *J. Fluid Mech.* **239**, 429–448.

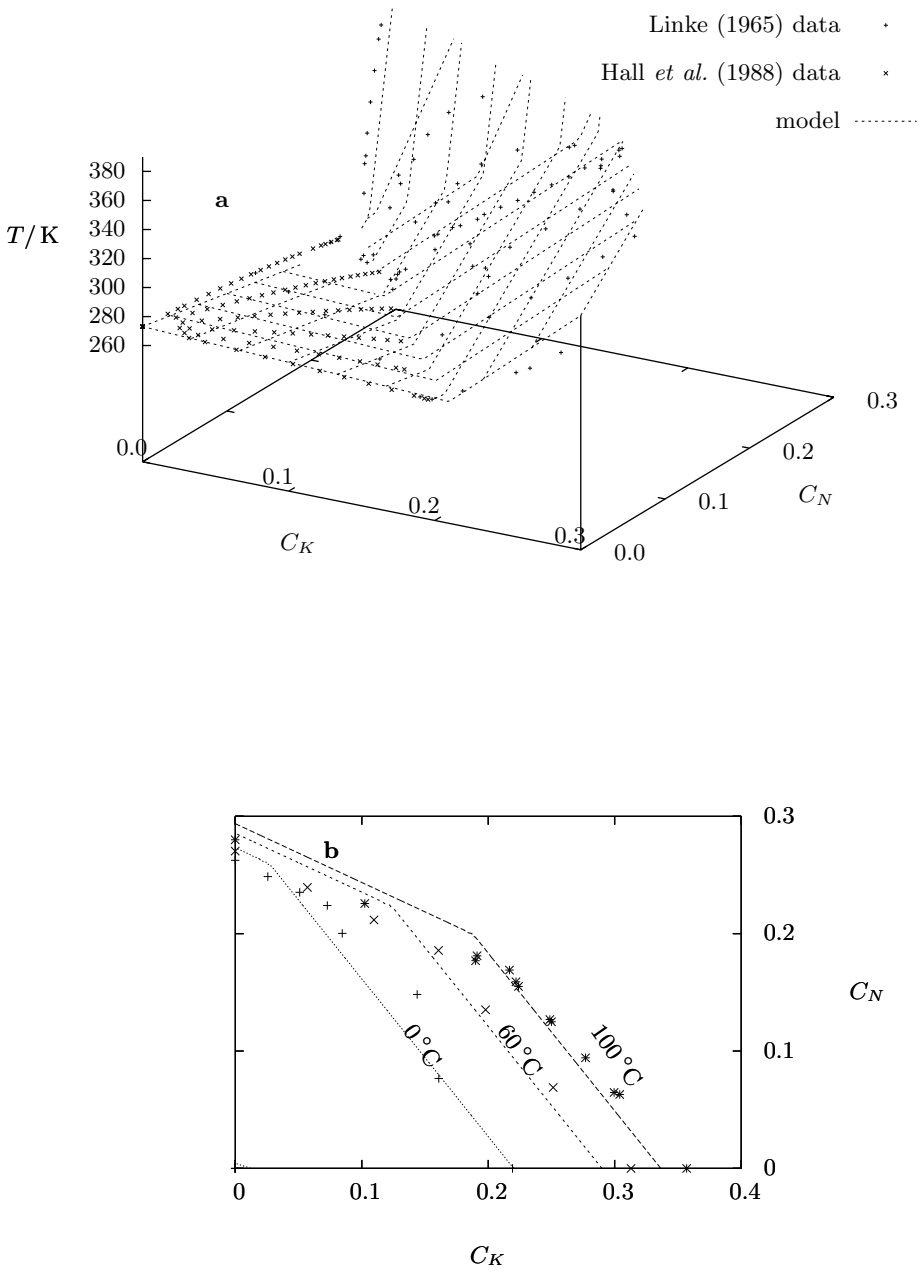

Figure 2. **a:** this graph shows phase-equilibrium data (crosses,) obtained from Linke (1965) and Hall *et al.* (1988), on a plot of temperature against KCl concentration and $NaCl$ concentration, along with the model in equation 2.6 (grid.) **b:** this graph shows temperature contours, in (KCl concentration, $NaCl$ concentration) space, in the model in equation 2.6 (lines,) and the empirical data points for temperatures within 1 °C either side of each contour temperature (crosses.)

Parameter	Value/ K	Parameter	Value
a_A	859.8	R	1.19
b_A	639.6	K_L	0.130 (0.561 W/ m/ K)
c_A	−83.9	K_S (solid KCl)	0.0199 (6.95 W/ m/ K)
a_B	2443.2	K_S (solid $NaCl$)	0.0273 (5.02 W/ m/ K)
b_B	4875.9	l_A	301 K
c_B	1059.1	l_B	18.1 K
a_I	−44.0	l_I	142 K
b_I	−122.68	r_{LS} (solid KCl)	0.559
c_I	−273.67	r_{LS} (solid $NaCl$)	0.512

Table 1. *This table shows numerical values of parameters used in the model. On the left are phase-equilibrium parameters obtained by fitting equation 2.6 to the data in figure 2a, while on the right are parameters obtained directly from the literature (Clauser & Huenges, 1995; Lewis[Peggs], 1995; Richardson, 1995; Morrell, 1995; Phillips, 1995a,b; McGlashan, 1995b,a; Marliacy et al., 1998; Wheeler & Newman, 2004; Ramos et al., 2005). Salt A is KCl and salt B is $NaCl$. Thermal conductivities underlying K_L and K_S values are in brackets.*

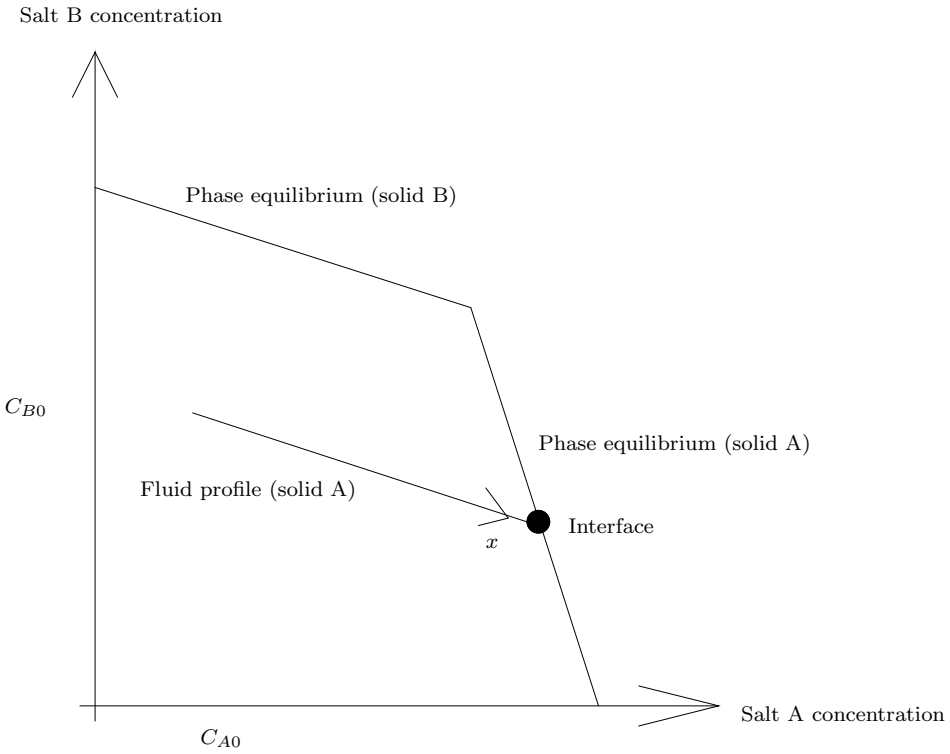

Figure 3. This cartoon illustrates the phase-equilibrium surface from figure 2, and the simultaneous spatial variation of the two salt concentrations, emphasizing that fluid is constrained to be in phase equilibrium where it meets solid. The arrow-head on the profile indicates the direction of increasing position co-ordinate x.

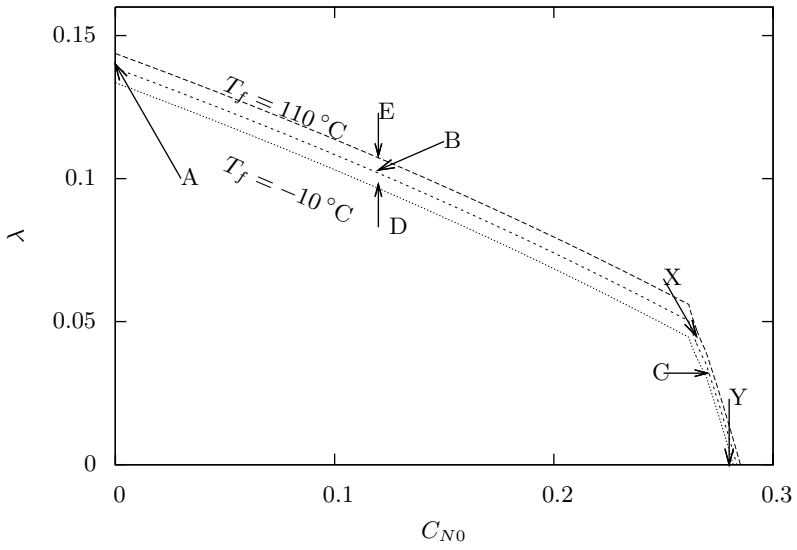

Figure 4. This graph shows predictions for the dissolution rate of solid KCl ($k = K$,) as a function of $NaCl$ concentration in the far-field brine; C_{N0} represents the externally-imposed concentration of the far-field brine, not the local concentrations influenced by the dissolving solid. Three curves are plotted, corresponding to far-field brines at $T_f = -10\,^\circ$C, $T_f = 50\,^\circ$C, and $T_f = 110\,^\circ$C. Throughout, the KCl concentration of the far-field brine is $C_{K0} = 0$, and the far-field solid temperature is $T_s = 50\,^\circ$C.

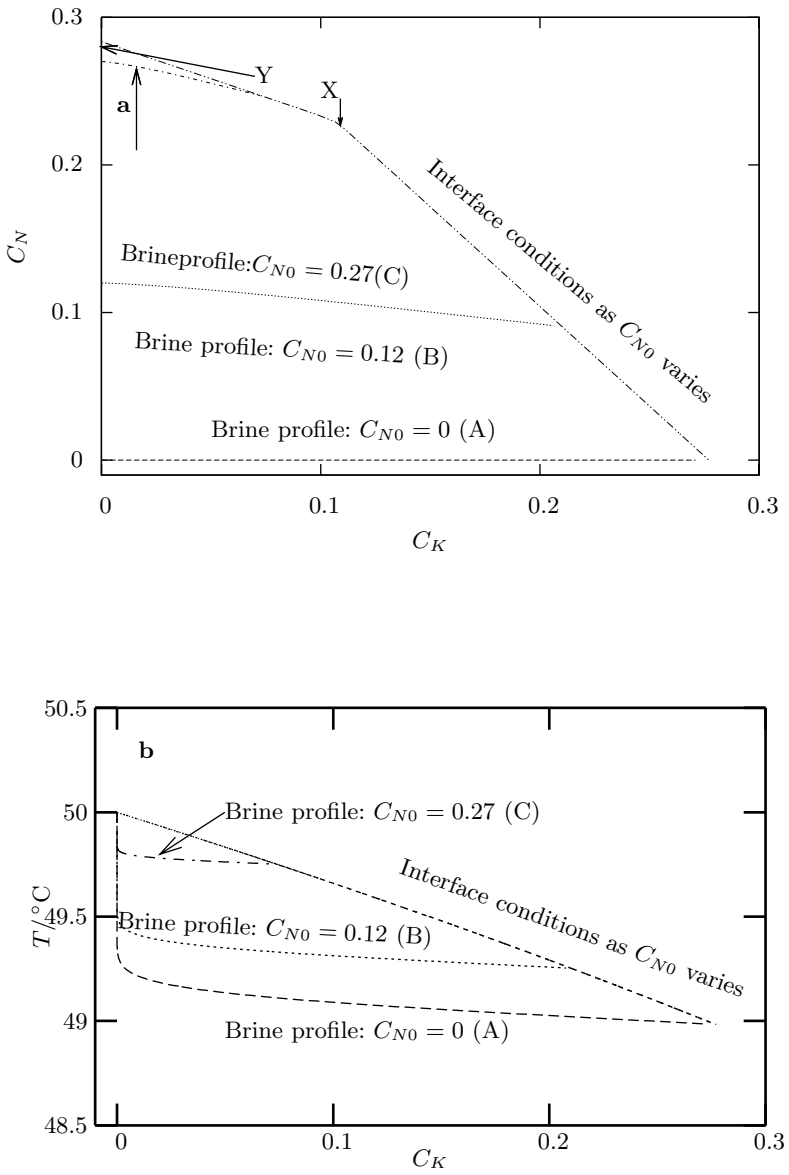

Figure 5. **a:** this graph shows predicted KCl concentration-$NaCl$ concentration profiles of the brine, for three far-field brine $NaCl$ concentrations (A, B, and C in figure 4,) and the predicted KCl concentration-$NaCl$ concentration space locus of interface brine conditions, as C_{N0} varies. **b:** this graph shows predicted KCl concentration-temperature profiles of the brine, for three far-field $NaCl$ concentrations (A, B, and C in figure 4,) and the predicted KCl concentration-temperature space locus of interface conditions, as C_{N0} varies. **Both panels:** the only solute in the far-field brine is $NaCl$ ($C_{K0} = 0$.) The solid is KCl ($k = K$.) The far-field temperatures are $T_f = T_s = 50\,^{\circ}\mathrm{C}$.

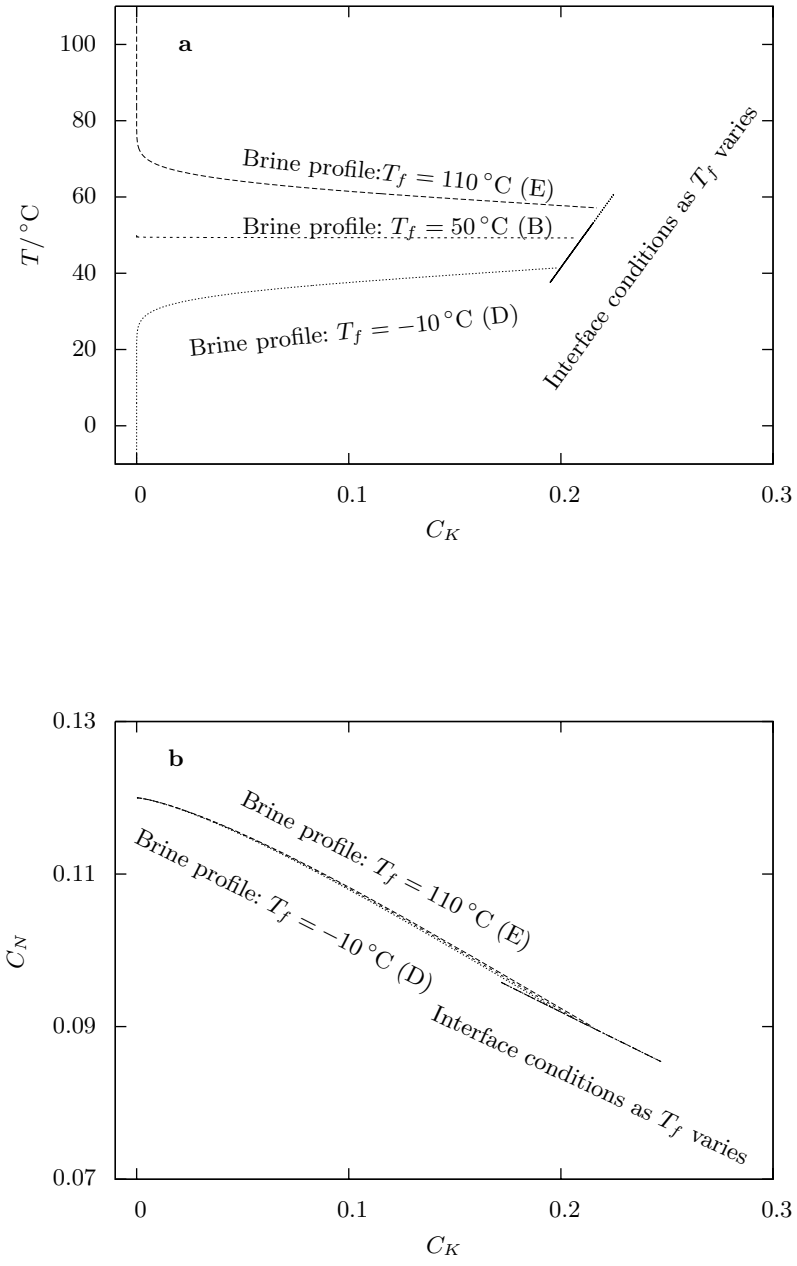

Figure 6. **a:** this graph shows predicted KCl concentration-temperature profiles of the brine, for three far-field brine temperatures (points D, B, and E in figure 4,) along with the predicted locus, in KCl concentration-temperature space, of interface brine conditions, as T_f varies. **b:** this graph shows predicted KCl concentration-$NaCl$ concentration profiles of the brine, for three far-field brine temperatures (points D, B, and E in figure 4,) along with the predicted locus, in KCl concentration-$NaCl$ concentration space, of interface brine conditions, as T_f varies. **Both panels:** the only solute in the far-field brine is $NaCl$ ($C_{K0} = 0$.) The solid is KCl ($k = K$.) The far-field brine $NaCl$ concentration $C_{N0} = 0.12$ and the far-field solid temperature $T_s = 50\,^\circ$C.

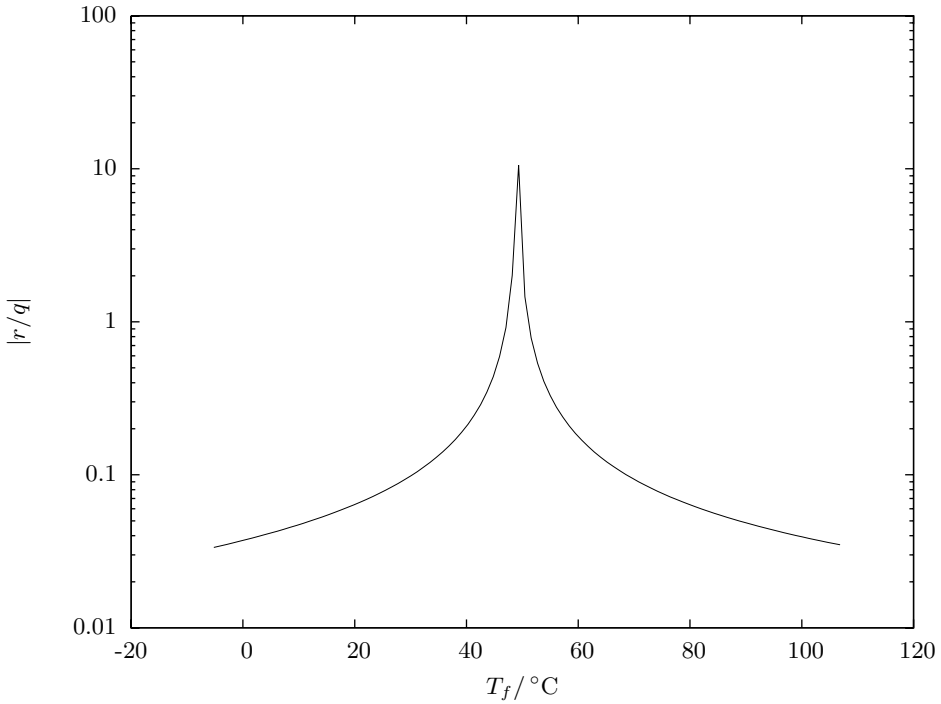

Figure 7. This graph shows the modulus of the predicted ratio of the heat flux r used as latent heat, to achieve dissolution, to the heat flux q delivered from the brine to the interface, as a function of far-field brine temperature. The solid is KCl ($k = K$.) The only solute in the far-field brine is $NaCl$ ($C_{K0} = 0$.) The far-field brine $NaCl$ concentration is fixed at $C_{N0} = 0.12$, and the far-field solid temperature is fixed at $T_s = 50\,^{\circ}\mathrm{C}$. It is interesting to note the sign of r/q: to the left of the peak, $q < 0$ (and therefore $r/q < 0$,) i.e. heat is transported from the interface to the far-field fluid, while to the right of the peak, $q > 0$ (and therefore $r/q > 0$,) i.e. heat is transported from the far-field fluid to the interface.

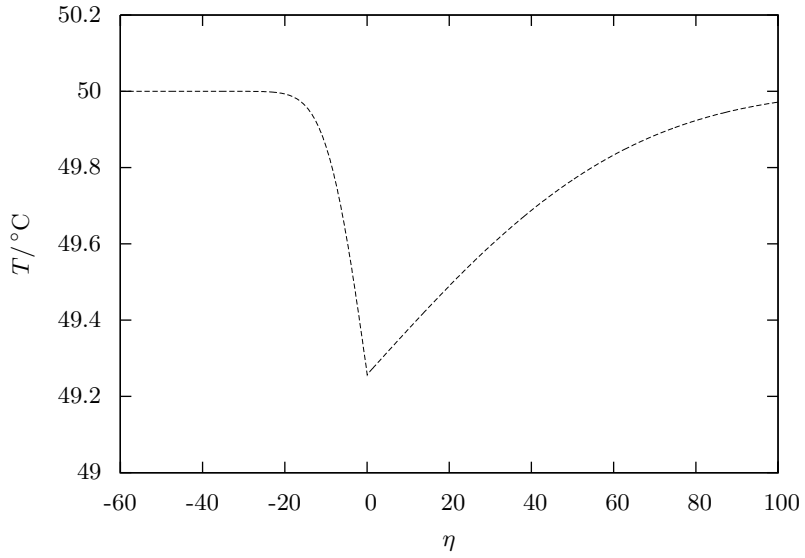

Figure 8. This graph shows the predicted variation of temperature with position in the brine, for far-field brine temperature $T_f = 50\,^{\circ}\mathrm{C}$ (point B in figure 4.) The only solute in the far-field brine is $NaCl$ ($C_{K0} = 0$.) The solid is KCl ($k = K$.) The far-field brine $NaCl$ concentration $C_{N0} = 0.12$, and the far-field solid temperature $T_s = 50\,^{\circ}\mathrm{C}$. The dimensionless position variable η becomes more positive on moving away from the far-field fluid, towards the far-field solid.

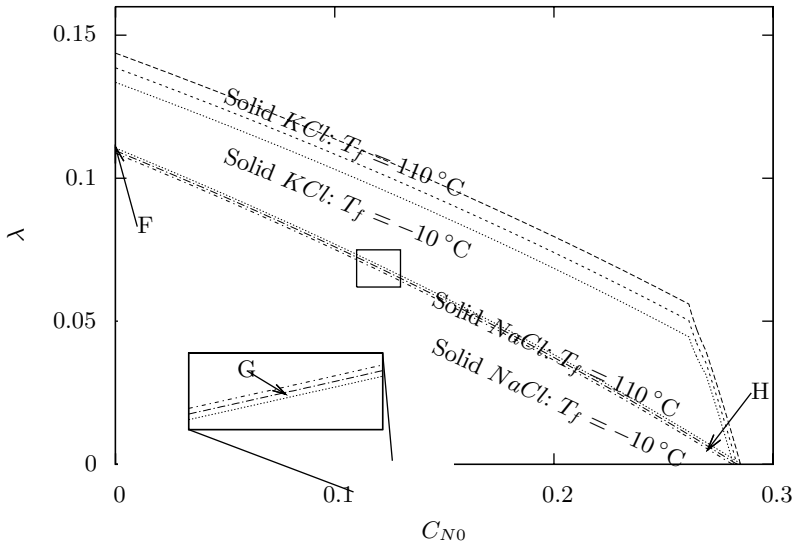

Figure 9. This graph compares predictions (cf. figure 4,) for the dissolution rate of solid KCl ($k = K$,) as a function of $NaCl$ concentration in the far-field brine (solid lines,) with predictions for the dissolution rate of solid $NaCl$ ($k = N$,) as a function of $NaCl$ concentration in the far-field brine (broken lines.) For each solid, three curves are plotted, corresponding to far-field brines at $T_f = -10\,^\circ$C, $T_f = 50\,^\circ$C, and $T_f = 110\,^\circ$C. Throughout, the KCl concentration of the far-field brine is $C_{K0} = 0$, and the far-field solid temperature is $T_s = 50\,^\circ$C.

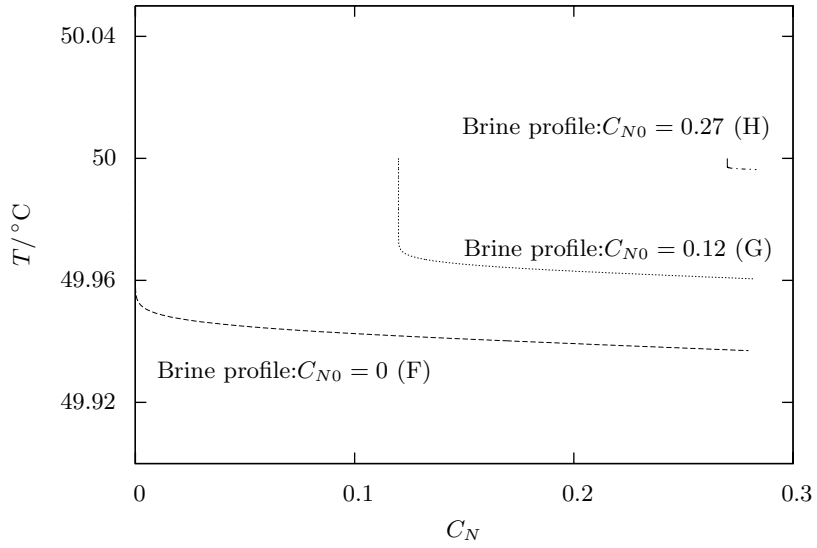

Figure 10. This graph shows predicted $NaCl$ concentration-temperature profiles of the brine, for three far-field brine $NaCl$ concentrations (points F, G, and H in figure 9.) The only solute in the far-field brine is $NaCl$ ($C_{K0} = 0$,) and the solid is $NaCl$ ($k = N$.) The far-field temperatures are $T_f = T_s = 50\,^{\circ}\mathrm{C}$

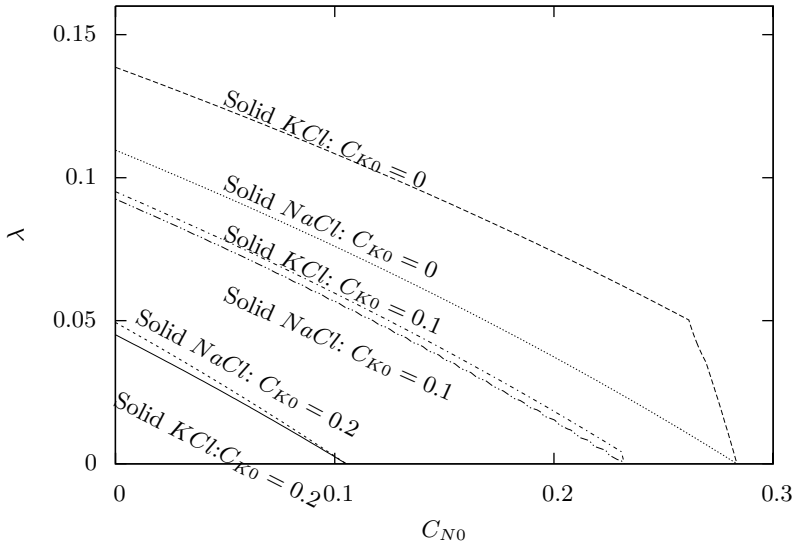

Figure 11. This graph shows predictions for the dissolution rates of both solid KCl (i.e. $k = K$) and solid $NaCl$ (i.e. $k = N$,) as functions of $NaCl$ concentration in the far-field brine. For each solid, three curves are plotted, corresponding to far-field brines with KCl concentration $C_{K0} = 0$, $C_{K0} = 0.1$, and $C_{K0} = 0.2$. Throughout, the far-field temperatures are $T_f = T_s = 50\,^{\circ}\mathrm{C}$.